Tunable Talbot imaging distance using an array of beam-steered metamaterial leaky-wave antennas

J. S. Gómez-Díaz,[1,a)] A. Álvarez-Melcón,[1] S. Gupta,[2] and C. Caloz[2]
[1]*Technical University of Cartagena, Campus Muralla del Mar-Antiguones, Cartagena (Murcia), Spain*
[2]*École Polytechnique de Montréal, 2500, ch. de Polytechnique, Montreal, Quebec H3T 1J4, Canada*

(Received 19 February 2009; accepted 7 August 2009; published online 29 October 2009)

A tunable spatio-temporal Talbot imaging phenomenon is presented. This phenomenon is based on the radiation properties of an array of beam-steered metamaterial composite right-/left-handed leaky-wave antennas, which is excited by a modulated pulse. The scanning law property of these antennas is exploited to achieve off-axis radiation, which leads to a tunable Talbot distance, as a function of the input pulse modulation frequency. The proposed Talbot phenomenon is analyzed theoretically, taking into account the aberrations produced by higher-order terms present in the free-space transfer function. Numerical simulations confirm the self-imaging and pulse multiplication effects and their tunability capabilities as a function of frequency. Finally, the experimental results are included to confirm the phenomenon predicted. © *2009 American Institute of Physics*. [doi:10.1063/1.3213382]

I. INTRODUCTION

The Talbot phenomenon was discovered by Talbot in 1836.[1] It occurs when a monochromatic wave is transmitted through (or reflected from) a periodically distributed spatial object. An exact image of the original object appears at a specific distance (called the Talbot distance, z_T) and additional images, with a period multiple of the original object period, appear at fractional distances of z_T. Thanks to the mathematical equivalence between the paraxial Fresnel approximation and the temporal propagation in first-order dispersive medium, the Talbot effect possesses a temporal counterpart.[2] In this case, an input pulse train is exactly replicated along the medium at the Talbot distance, and a multiplication of the repetition rate of the periodic signal is observed at fractional Talbot distances.

The Talbot phenomenon has found a wide variety of applications, ranging from array illumination[3] or phase locking for laser arrays[4] to the multiplication of the repetition rate of a periodic pulse train[5] or pulse compression,[6] in optical fibers.

The spatio-temporal Talbot phenomenon[7] occurs when the elements of an array of composite right-/left-handed (CRLH)[8] metamaterial leaky-wave antennas (LWAs)[9] are simultaneously fed with a (single) modulated pulse. This effect is based on the combination of the conventional spatial monochromatic Talbot effect and the transient (polychromatic) character of the pulse radiation phenomenon in the LWA structure. The different spatial beams, which correspond to different temporal frequencies, interfere in space forming a self-imaging pattern constituted of narrow Talbot zones, due to the nonzero bandwidth of the input pulse.[7] Note that this configuration provides the regular Talbot phenomenon only when the array of CRLH LWAs are fed by a pulse modulated at the transition frequency (i.e., broadside radiation) of the antennas.

In this paper, the general situation of an array of CRLH LWAs fed by a pulse modulated at any frequency is studied, and a closed-form solution for the spatio-temporal Talbot distance is given. This distance is equal to that obtained in Ref. 7 for the case of broadside radiation (i.e., modulation frequency set to the transition frequency of the LWA). In addition, note that a change in the modulation frequency provides a variation in the radiation angle [due to the scanning law of the LWAs (Ref. 9)], which also contributes to modify the position of the Talbot distance. This change in the radiation angle can also be exploited to electronically tune the Talbot distance. Furthermore, an "aberration frequency region" for this phenomenon is defined when the modulation frequency is selected far from the transition frequency of the antenna. Aberrations arise due to higher-order terms of the channel transfer function and are more important as long as the difference between these two frequencies increases. This affects the self-imaging process, which is progressively distorted and finally destroyed.

A similar phenomenon, but for the monochromatic case, has been previously reported in the optical domain, using diffraction gratings.[10] In this case, the diffraction gratings are illuminated with an oblique plane wave. The behavior of the CRLH LWA (Ref. 8) in the microwave domain is similar to the diffraction gratings in optics but with several advantages. First, CRLH LWAs are simply fed by an input port. On the contrary, the feeding of the diffraction gratings is more complicated and requires an external device to generate a plane wave. This plane wave is then used to illuminate the diffraction gratings. Second, the CRLH LWA scanning law property[9] electronically performs an off-axis radiation. In the optical domain, the plane-wave generator must be mechanically rotated to achieve a similar type of off-axis radiation.[10] Third, the CRLH LWA is a periodic structure, where the length of the unit cell is electrically very small. Therefore, it does not suffer of spurious secondary lobes because it operates in the fundamental space harmonic, and the higher space

a)Electronic mail: jsebastian_gomez@ono.com.

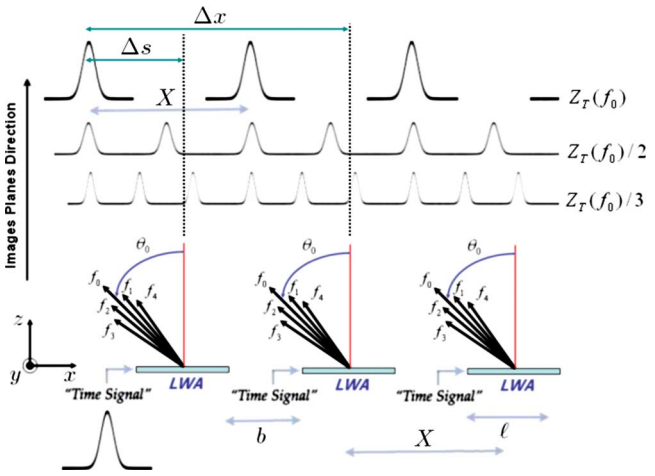

FIG. 1. (Color online) Proposed CRLH LWA array configuration for the investigation of the spatial-temporal Talbot effect. Each antenna radiates the different frequency components of the input modulated pulse to different angles of space. For the sake of simplicity, only the envelopes of the pulses at the main Talbot plane and two fractional Talbot planes are shown.

harmonics are very little excited. However, note that the spatio-temporal Talbot phenomenon is only achieved within a particular frequency range. If the phenomenon must be reproduced at a different range, the antennas of the array should be replaced by other antennas designed to operate at that frequency range.[8]

The tunable spatio-temporal Talbot phenomenon is numerically demonstrated using a time-domain Green's function approach.[11–13] The self-imaging and the pulse multiplication effects are shown within the tunable frequency region, and the aberrations which arise from off-axis radiation are studied. Finally, an experimental setup is used to demonstrate, for the first time, this Talbot phenomenon. Specifically, an array of seven CRLH LWAs is employed to reproduce this effect for the case of broadside radiation at the Talbot distance z_T (as was theoretically predicted in Ref. 7) and also for the case of off-axis radiation, at the fractional distance $z_T/2$, thereby validating the theory proposed in this paper.

II. TUNABLE SPATIO-TEMPORAL TALBOT DISTANCE

This section presents the detailed mathematical analysis of the spatial-temporal tunable Talbot distance, based on an array of beam-steered metamaterial LWAs.

Consider an infinite array of CRLH LWAs, with antenna element spacing b and element length ℓ, where all the elements are fed simultaneously with the same input pulse, as illustrated in Fig. 1. This pulse is modulated at the frequency ω_0 and, assuming the phasor time dependence $e^{+j\omega t}$, may be expressed as $\Psi(t)=\Psi_0(t)e^{j\omega_0 t}$, where $\Psi_0(t)$ is a slowly varying envelope and ω_0 is the modulation frequency. Due to the time independence of the Talbot distance,[7] the spatial distribution of the field along each CRLH array element, denoted by $A_e(x,z=0)$, is considered at the fixed time $t=t'$, which may be seen as a "snapshot" of the pulse along the element. Taking the spatial Fourier transform of the field along the overall array, we can write[1,7]

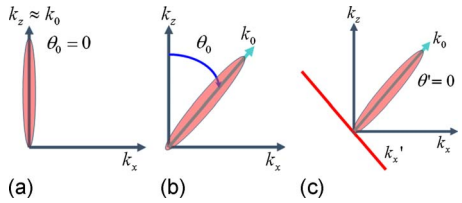

FIG. 2. (Color online) Steered beam radiation in the propagation plane. (a) Broadside radiation. (b) Radiation in arbitrary direction (off-axis radiation). (c) Definition of an auxiliary rotated reference system for the case of off-axis radiation.

$$\tilde{A}_a(k_x,z=0)=\Delta k_x \sum_{p=-\infty}^{+\infty} \tilde{A}_e(k_x=p\Delta k_x)\,\delta(k_x-p\Delta k_x), \qquad (1)$$

where $\Delta k_x=2\pi/X$ is the spatial repetition frequency and $X=b+\ell$ is the corresponding antenna element spacing (spatial period, see Fig. 1).

On the other hand, the transfer function of the CRLH LWA, assuming plane-wave propagation,[9] is given by[7,14]

$$\tilde{H}(k_x,z)=e^{-jk_z z}=e^{-j\sqrt{k_0^2-k_x^2}z}, \qquad (2)$$

where the Helmholtz equation implies the separability condition in the wavenumbers $(k_0^2=k_z^2+k_x^2)$.

The modulation frequency of the pulse controls the radiation angle (θ), following the CRLH LWA scanning law.[9] When this angle is different from 0°, an off-axis plane-wave propagation in the far field occurs. In this case, the spatial frequency is centered around this angle, following the law

$$k_x(\omega)=k_0 \sin\,\theta. \qquad (3)$$

To simplify Eq. (2), we can assume that the variation in the angle is relatively small over the frequency bandwidth of the pulse. In addition, due to the off-axis propagation, the radiation angle (θ) does not have any restriction. Specifically, it is not required that the radiation must be confined around the broadside direction $(\theta\neq 0°)$. The restriction $(\theta\approx 0°)$ was assumed in Ref. 7 to perform the paraxial approximation $[\sin(\theta)\approx\theta=k_x(\omega)/k_0]$. Therefore, the mathematical development presented in Ref. 7 cannot be used to characterize the more general situation treated in this paper.

At this point, we distinguish the radiation angle provided by the modulation frequency of the pulse, θ_0, and the angle variation provided by the pulse bandwidth, $\Delta\theta$. Taking this two independent contributions into account, the total radiation angle may be defined as

$$\theta(\omega)=\theta_0(\omega_0)+\Delta\theta(\Delta\omega). \qquad (4)$$

In order to compute the Talbot distance, a change in the coordinate system for the propagation constant is proposed. The idea is to approximate the relationship between the different propagation constants $[k_x(\omega)$ and $k_0]$ with the radiation angle provided by the pulse bandwidth. For this purpose, an auxiliary rotated coordinate system is defined as

$$k_x'(\omega)=k_x(\omega)-k_0 \sin\,\theta_0. \qquad (5)$$

This coordinate system depends on the modulation frequency of the input pulse, as graphically illustrated in Fig. 2.

Inserting Eq. (5) into Eq. (2), the transfer function of the channel becomes

$$\tilde{H}(k_x,z) = e^{-j\sqrt{k_0^2-k_x'^2-k_0^2\sin^2\theta_0+2k_x'k_0\sin\theta_0}z}, \tag{6}$$

which, for convenience, may be rewritten as

$$\tilde{H}(k_x,z) = e^{-jk_0\cos\theta_0\sqrt{1-2\sin\theta_0/\cos^2\theta_0(k_x'/k_0)-1/\cos^2\theta_0(k_x'/k_0)^2}z}. \tag{7}$$

According to the definition of k_x', an auxiliary radiation angle may be defined, using the CRLH LWA scanning law,[9] as

$$\theta' = \sin^{-1}\left[\frac{k_x'(\omega)}{k_0}\right]. \tag{8}$$

Independent of the actual radiation direction, for narrow beamwidths, we can assume $k_x' \approx 0$, so the ratio k_x'/k_0 is small, and the following approximation holds:

$$\theta' \approx \frac{k_x'(\omega)}{k_0}. \tag{9}$$

In addition, the square root of Eq. (7) may be approximated using the following Taylor series expansion:

$$\sqrt{1-x} \approx 1 - \frac{x}{2} - \frac{x^2}{8} - \frac{x^3}{16} \tag{10}$$

as

$$\sqrt{1-2\frac{\sin\theta_0}{\cos^2\theta_0}\theta' - \frac{1}{\cos^2\theta_0}\theta'^2} \approx 1 - \frac{\sin\theta_0}{\cos^2\theta_0}\theta' - \frac{1}{2\cos^4\theta_0}\theta'^2 - \frac{\sin\theta_0}{2\cos^6\theta_0}\theta'^3 - \frac{5\sin^2\theta_0+1}{8\cos^6\theta_0}\theta'^4 - \frac{3\sin\theta_0}{8\cos^6\theta_0}\theta'^5 - \frac{1}{\cos^6\theta_0}\theta'^6. \tag{11}$$

Note that due to the off-axis radiation, the different components of the Taylor expansion strongly depend on the angle θ_0, whereas they are constant in the case of broadside (not off-axis) radiation.[7] In addition, the terms depending on θ'^N, with $N \geq 3$, correspond to aberrations. These terms were not present at the broadside case (see Ref. 7) and contribute to distort the self-imaging process. Since $\theta' \approx 0$, the first aberration term (depending on θ'^3) is enough for an accurate characterization of these distortion phenomena. With these consideration, the transfer function of the channel is simplified to

$$\tilde{H}(k_x,z) = e^{-jk_0[\cos\theta_0-\tan(\theta_0)\theta'-(1/2\cos^3\theta_0)\theta'^2-(\sin\theta_0/2\cos^5\theta_0)\theta'^3]z}. \tag{12}$$

Next, the auxiliary angle θ' is linearized around the modulation frequency,[7]

$$\theta' \approx \xi(\omega-\omega_0), \tag{13}$$

where the linearization parameter ξ is defined as[7]

$$\xi = \left.\frac{\partial\theta'}{\partial\omega}\right|_{\omega=\omega_0} = \frac{\partial}{\partial\omega}\left(\frac{k_x'}{k_0}\right) = \frac{c}{\omega_0}\frac{1}{v_g'(\omega_0)}, \tag{14}$$

where $v_g'(\omega_0)$ is the group velocity related to the rotated k_x' propagation constant. Introducing the following relationship between the spatial and temporal frequencies:[7]

$$v_g(\omega_0)(k_x'-k_{x_0}) \approx (\omega-\omega_0), \tag{15}$$

the angle θ' may be defined as

$$\theta' = \xi v_g'(\omega_0)(k_x'-k_{x_0}) = \frac{c}{\omega_0}(k_x'-k_{x_0}). \tag{16}$$

Therefore, the transfer function of the channel in the rotated coordinate system, $\tilde{H}(k_x',z)$, may be expressed as

$$\tilde{H}(k_x,z) = \exp\left\{-j\left[\frac{\omega_0}{c}\cos\theta_0 - \tan\theta_0(k_x'-k_{x_0}) - \frac{1}{2\cos^3(\theta_0)}\frac{c}{\omega_0}(k_x'-k_{x_0})^2 - \frac{\sin\theta_0}{2\cos^5\theta_0}\frac{c^2}{\omega_0^2}(k_x'-k_{x_0})^3\right]z\right\}. \tag{17}$$

In order to derive the Talbot distance, only the third expansion term of the exponential is considered. Note that the first two terms do not provide any information on the Talbot distance.[7] The first term is related to the modulation frequency of the pulse and does not carry any information about the envelope, and the second term represents a k_x'-linear phase factor, equivalent in the spatial-temporal domain to the retarded frame in the time domain. In addition, a fourth term appears in this case, due to the off-axis radiation. This term does not contribute to the self-imaging process, but it is responsible for additional aberrations. Specifically, the self-imaging process occurs without an important distortion within the following angle region:[10]

$$-25^\circ < \theta < 25^\circ. \tag{18}$$

This range is an approximation, which assumes that the aberration terms are negligible inside that region. However, these terms are present at all angles (except broadside) and they will always cause a deviation from the ideal self-imaging process.[10] Note that this angle region does not depend on the separation distance between two consecutive antennas and that, due to the LWA scanning law, leads to different allowed frequency regions for the input pulse, as a function of the particular type of CRLH LWA employed. In addition, note that due to the scanning law of the CRLH LWA,[9] angles outside the allowed region can be achieved with frequencies higher or lower than the CRLH transition frequency. Therefore, at any other modulation frequency (higher or lower), the aberration terms appear and increase their influence as long as the modulation frequency differs from the CRLH transition frequency.

With the above simplifications and considerations, the transfer function of the system, outside the aberration frequency region, may be rewritten around k_{x_0} as

$$\tilde{H}(k_x^T,z)=\tilde{H}(k_x'=k_{x_0}+k_x^T,z)=e^{j(k_0/2\cos^3(\theta_0))(c^2/\omega_0^2)(k_x^T)^2 z}. \tag{19}$$

Combining Eq. (1) and Eq. (19), the output signal radiated at the distance z is expressed in the transformed domain as

$$\begin{aligned}\tilde{A}_r(k_x^T,z)&=\tilde{A}_a(k_x^T,z=0)\tilde{H}(k_x^T,z)\\&=\Delta k_x\sum_{p=-\infty}^{+\infty}\tilde{A}_e(p\Delta k_x)\delta(k_x^T-p\Delta k_x)\tilde{H}(k_x^T,z)\\&=\Delta k_x\sum_{p=-\infty}^{+\infty}\tilde{A}_e(p\Delta k_x)\delta(k_x^T-p\Delta k_x)e^{jp^2\phi},\end{aligned} \tag{20}$$

where

$$\phi=\frac{k_0}{2\cos^3(\theta_0)}\frac{c^2}{\omega_0^2}\Delta k_x^2 z. \tag{21}$$

If the condition

$$p^2\phi=2\pi q'=2\pi q p^2, \tag{22}$$

with $q,q'\in\mathbb{N}$ (q' varies with p but q is constant), is satisfied, the phase factor in Eq. (20) reduces to unity, so that $\tilde{A}_r(k_x',z)\propto\tilde{A}_a(k_x',z=0)$ according to Eq. (1), i.e., the field distribution at z (output) is an exact replica of the field distribution at $z=0$ (input). Therefore, the distance z is the integer Talbot distance, which using $\Delta k_x=2\pi/X$ yields

$$z_t=\frac{2q'X^2}{\lambda_0}\cos^3\theta_0. \tag{23}$$

Some clarifications are needed regarding this tunable Talbot distance. First, additional control over the regular Talbot distance[1,2,7] is provided. This may be exploited to tune the position of the Talbot distance, taking advantage of the CRLH LWA scanning law. Second, the new Talbot distance expression directly depends on the radiation angle (θ_0). This behavior is similar to that of a diffraction grating in the optical domain, when illuminated by an oblique plane wave.[10] However, in our case, it is the scanning behavior of the CRLH LWA which provides off-axis radiation as a function of frequency. Therefore, it is not required to mechanically rotate a plane-wave generator, as in other optical applications. Third, note that the scanning law depends on the propagation constant of a particular CRLH element (see Ref. 9). Therefore, the tunability of the Talbot distance can also be controlled using a particular antenna with a different scanning law. For the case of broadside radiation, which is common to all antennas and is obtained when the input pulse modulation frequency is set to the CRLH transition frequency, the tunable Talbot distance reduces to the well-known Talbot distance[1,7]

$$z_t=\frac{2q'X^2}{\lambda_0}. \tag{24}$$

Note that when the modulation frequency of the input pulse is different from the CRLH transition frequency,[8] a spatial shift at the Talbot planes occurs. This spatial shift is due to the off-axis propagation, which induces a lateral shift of the entire radiation given by

$$\Delta x=z_T(f_0)\tan\theta_0. \tag{25}$$

Finally, it is important to mention that the main contribution to the Talbot distance tunability is due to the change in the frequency itself. However, the frequency change also introduces a variation in the radiation angle, which further modifies the Talbot distance [see Eq. (23)] and must rigorously be taken into account for practical designs. In addition, note that the self-imaging process obtained using the off-axis radiation of CRLH LWA is not ideal. This is due to the aberrations found in the description of the free-space transfer function, which cause deviation from the ideal reconstruction of the pulses. The influence of these aberrations is small within the allowed angle region [Eq. (18)], but it is always present. Moreover, the narrow-band assumption employed for the paraxial approximation[7] and the use of a finite number of antennas for practical cases also contribute to degrade the quality of the recomposed pulses at the Talbot distance.

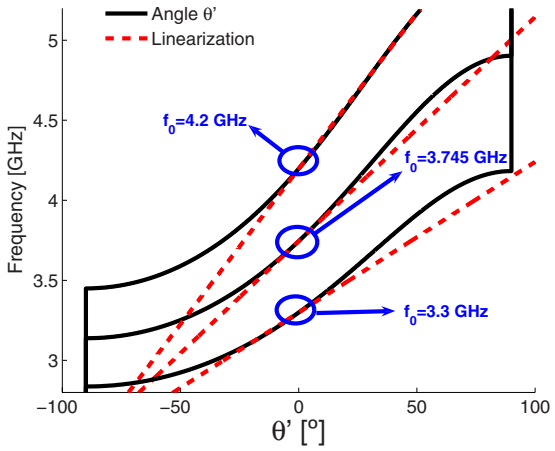

FIG. 3. (Color online) Linearization of the rotated auxiliary angle θ' around broadside ($\theta'=0$) for different modulation frequencies of the input pulse, computed using Eq. (13).

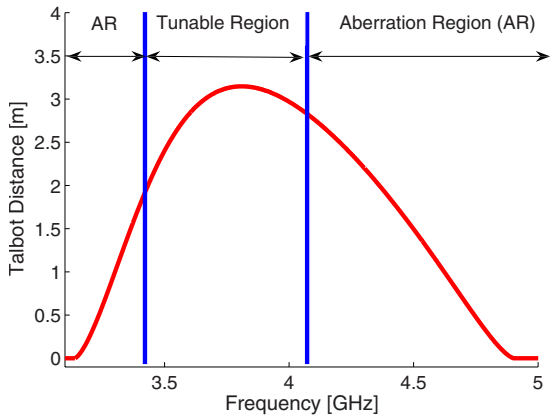

FIG. 4. (Color online) Tunable spatial-temporal Talbot distance as a function of frequency, computed with Eq. (23). The circuit parameters of the CRLH LWA employed are $C_R=1.29$ pF, $C_L=0.602$ pF, $L_R=3.0$ nH, and $L_L=1.4$ nH, and the separation distance between two consecutive antennas is $b=38.80$ cm.

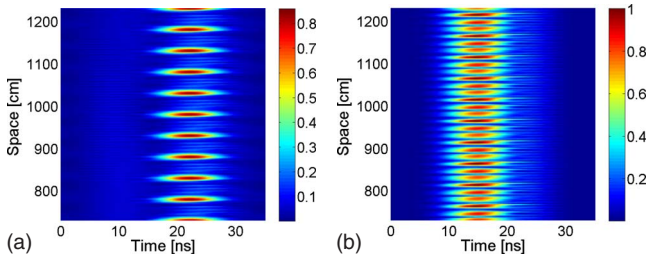

FIG. 5. (Color online) Field (magnitude) radiated by a CRLH LWA array excited by an input pulse with a modulation frequency of $f_0=3.745$ GHz at two different propagation distances (z-axis): (a) $z=z_t=3.1208$ m and (b) $z=z_t/3=1.0403$ m.

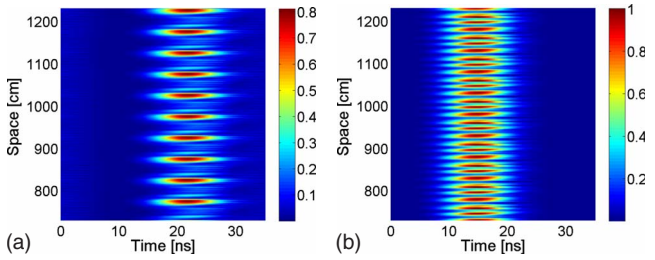

FIG. 7. (Color online) Field (magnitude) radiated by a CRLH LWA array excited by an input pulse with a modulation frequency of $f_0=4.0$ GHz at two different propagation distances (z-axis): (a) $z=z_t=2.926$ m and (b) $z=z_t/3=0.9753$ m.

III. SIMULATION RESULTS

This section presents simulation results to demonstrate the tunability of the spatio-temporal Talbot phenomenon. For this purpose, an exact time-domain Green's function approach is employed.[11–13] The CRLH LWA used in the array is composed of $N=14$ unit cells of length $p=0.8$ cm ($\ell=Np$), with the circuital parameters $C_R=1.29$ pF, $C_L=0.602$ pF, $L_R=3.0$ nH, and $L_L=1.4$ nH, corresponding to a transition frequency of $f_0=3.745$ GHz.[8] Each antenna is excited by an f_0-modulated Gaussian pulse with full width at half maximum of 3.5 ns. In addition, the radiation of an array composed of 50 elements is considered. This simulates an infinite array around the ten central antennas, where the results will be discussed.

The use of the rotated auxiliary propagation constant k_x' provides a fix radiation around the direction ($\theta'\approx 0$), independent of the input pulse modulation frequency. For this purpose, k_x' is dynamically changed as a function of this modulation frequency [Eq. (5)]. This effect can be observed in Fig. 3, where the auxiliary angle θ', defined in Eq. (8), is shown for different modulation frequencies (at broadside, backward, and forward).

This angle is then linearized around $\theta'=0°$, using Eq. (16). Note that, although in all cases $\theta'=0°$, the actual radiation direction (θ) changes with the modulation frequency. The linearization procedure provides the paraxial approximation employed for the definition of the tunable Talbot distance. Since it is only valid in the frequency region around $\theta'\approx 0°$, the subsequent mathematical derivations are only valid for the case of narrow-band pulses.[7]

Figure 4 presents the tunable Talbot distance as a function of the input pulse modulation frequency, when the antenna elements spacing is set to $X=0.5$ m.

As it was discussed in Sec. II, two frequency regions are clearly observable. The first region, denoted as "tunable region," is limited by the allowed angle region of Eq. (18), which is translated into frequency through the CRLH LWA scanning law [Eq. (3)]. Within this region, the influence of higher-order terms present in the channel transfer function is not very important and can be neglected. In the second region, denoted as "aberration region (AR)," the influence of these terms destroy the self-imaging process and limit the useful frequency region of the tunable spatio-temporal Talbot phenomenon.

In order to validate the proposed analytical approach, the magnitude of the field radiated by an array of 50 LWAs at the z_T and $z_T/3$ positions will be shown as a function of the x-axis and of time. For the sake of clarity, only the region of the ten central antennas is presented. In Fig. 5, the modulation frequency of the input pulse is set to the transition frequency of the CRLH ($f_0=3.745$ GHz) which corresponds to broadside radiation. In this case, the influence of the high-order terms is small, leading to a high-quality reconstruction of the pulses, even at the fractional Talbot distance $z_T/3$.

In Figs. 6 and 7, the modulation frequency is set to $f_0=3.5$ GHz (corresponding to backward radiation) and to $f_0=4.0$ GHz (corresponding to forward radiation), respectively. In both cases, the self-imaging phenomenon occurring at the Talbot distance and the pulse multiplication effect occurring at the fractional Talbot distance $z_T/3$ can clearly be observed. However, the reconstruction in this case is not as good as in the case of broadside radiation (see Fig. 5), and

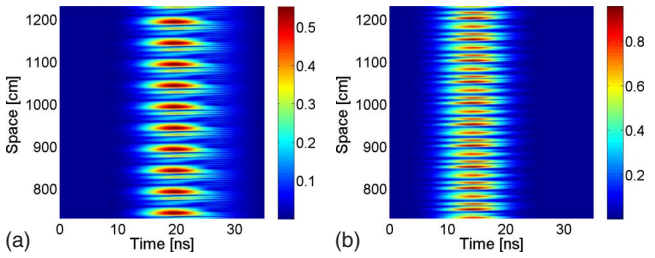

FIG. 6. (Color online) Field (magnitude) radiated by a CRLH LWA array excited by an input pulse with a modulation frequency of $f_0=3.5$ GHz at two different propagation distances (z-axis): (a) $z=z_t=2.430$ m and (b) $z=z_t/3=0.8100$ m.

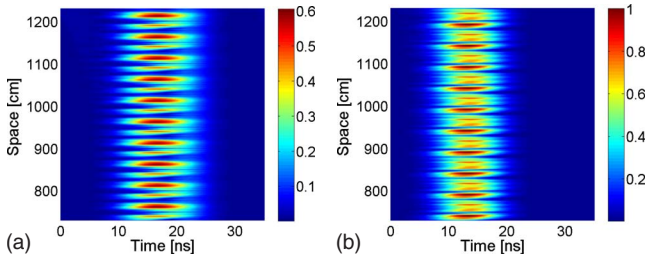

FIG. 8. (Color online) Field (magnitude) radiated by a CRLH LWA array with infinite number of elements excited by an input pulse with a modulation frequency of $f_0=3.3$ GHz at two different propagation distances (z-axis): (a) $z=z_t=1.103$ m and (b) $z=z_t/3=0.3677$ m.

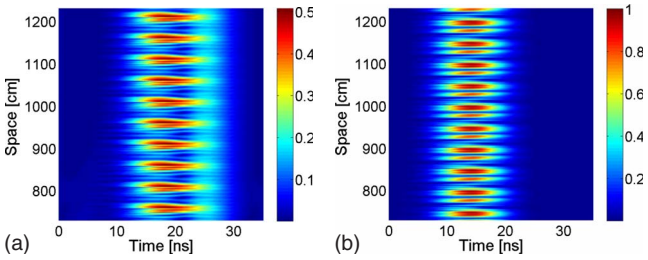

FIG. 9. (Color online) Field (magnitude) radiated by a CRLH LWA array excited by an input pulse with a modulation frequency of f_0=4.5 GHz at two different propagation distances (z-axis): (a) $z=z_t$=1.221 m and (b) $z=z_t/3$=0.4070 m.

small distortions and very low-level secondary pulses come out. This is due to the higher-order terms of the channel transfer function, which appear in the off-axis radiation case, degrading the self-imaging process. However, since we are operating in the tunable region of the Talbot distance (see Fig. 4), the influence of these terms is not strong enough to destroy the Talbot phenomena.

In Figs. 8 and 9, the modulation frequency is set to f_0 =3.3 GHz (corresponding to backward radiation) and to f_0 =4.5 GHz (corresponding to forward radiation), respectively. Note that in this case the modulation frequencies employed are in the aberration region, out of the allowed angle range defined by Eq. (18). As can be seen in these figures, the self-imaging process is not very clear, and the pulses are reconstructed with distortion at the Talbot distance z_T. In the same way, the multiplication pulse effect, which should occur at the fractional distance $z_T/3$, is also destroyed.

Finally, note that a shift in space occurs as a function of the input pulse modulation frequency, following Eq. (25). However, taking into account that an infinite (or high enough) number of antennas is considered in the simulations, this shift is not really visible. In fact, in this case only a small shift of the pulses position over the antenna appears (see Fig. 1). This shift, denoted Δs, may be calculated as

$$\Delta s = \Delta x - nX, \tag{26}$$

where $n \in \mathbb{N}$ is the largest natural number which keeps Δs positive. For the examples presented in this section, these

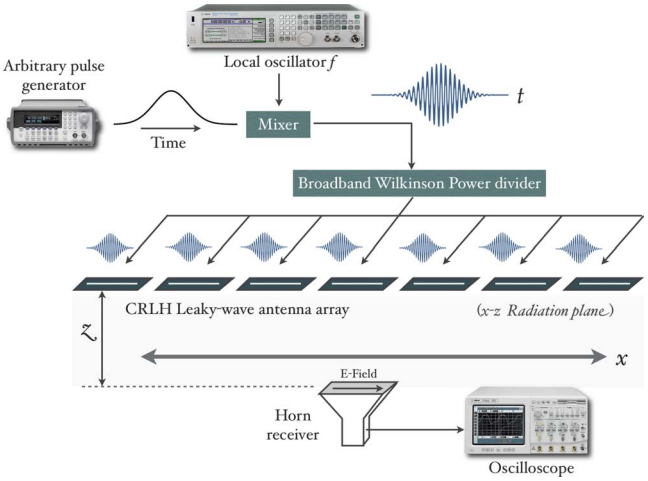

FIG. 10. (Color online) Schematic diagram of the proposed experimental setup employed to reproduce the tunable spatio-temporal Talbot phenomenon.

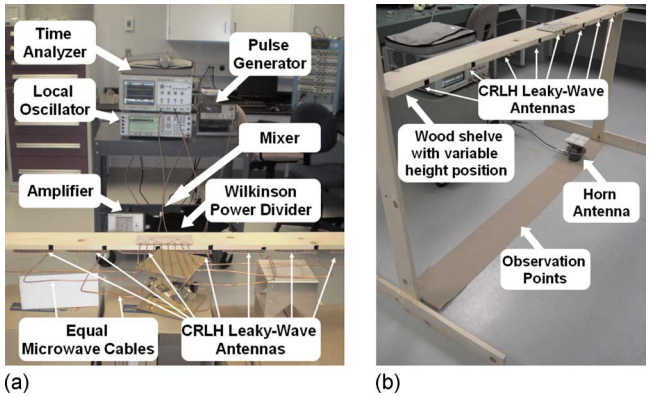

FIG. 11. (Color online) Overview of the entire setup and equipment employed to reproduce the spatio-temporal Talbot phenomenon. (a) Generation, distribution, and radiation of the modulated pulses. (b) Radiation and reception of the modulated pulses.

variations yield Δs=0.4083, 0.3641, 0.0, 0.3935, 0.0822 m, corresponding to the modulation frequencies f_0 =3.3, 3.5, 3.745, 4.0, 4.5 GHz, respectively. For instance, consider the pulse located around 783.1 cm for the case of broadside radiation at z_T [see Fig. 5(a)]. When the modulation frequency is changed to f_0=3.5 GHz, the CRLH LWAs begin to radiate at a backward direction. Therefore, that particular pulse is shifted down to a space position around 743.0 cm (see Fig. 6), following the space variation predicted with Eq. (26).

IV. EXPERIMENTAL RESULTS

This section presents, for the first time, an experimental demonstration of the spatio-temporal Talbot effect. Specifically, this phenomenon has been validated for the case of broadside radiation at the Talbot distance z_T (as it was theoretically predicted in Ref. 7) and also for the case of off-axis radiation, at the fractional distance $z_T/2$, therefore validating the theory proposed in Sec. II.

A diagram of the configuration employed to reproduce the spatio-temporal Talbot phenomenon is sketched in Fig. 10. In addition, a picture of the experimental setup is shown

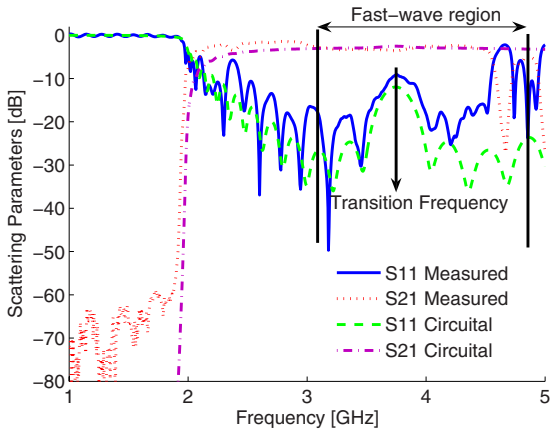

FIG. 12. (Color online) Scattering parameters of a single CRLH LWA employed to reproduce the spatio-temporal Talbot phenomenon, obtained using circuit analysis (Ref. 8). Measured data are employed for validation purposes.

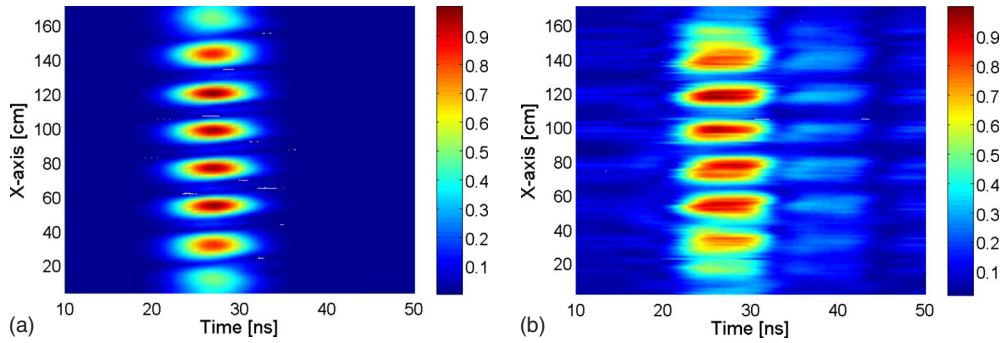

FIG. 13. (Color online) Normalized field (magnitude) radiated by an array of seven CRLH LWAs elements, excited by an input pulse with a modulation frequency $f_0=3.745$ GHz at the Talbot distance of $z_T=0.5483$ m. (a) Simulation results. (b) Measured data.

in Fig. 11.

The setup is composed of an arbitrary baseband pulse generator, which provides a Gaussian pulse. This pulse is then up-converted in frequency using a microwave mixer and a local oscillator. The modulated pulse goes through a Wilkinson power divider,[15] which provides seven identical outputs. Next, seven identical microwave cables are employed to carry the modulated signals to the CRLH LWAs. This step is very important because a small difference in the cable length may destroy the synchronization required to reproduce the phenomenon. The array of seven CRLH LWAs, with an antenna element spacing of $X=22$ cm, simultaneously radiates the modulated pulses. Note that a single CRLH LWAs can be described with the circuit parameters employed in the simulation results of Sec. II. This is demonstrated in Fig. 12, where a comparison between measured and simulated scattering parameters is presented.

As it can be seen in Fig. 11, the array of antennas is placed in a wood shelve which can vary its position in height. Therefore, it is simple to place the array at several planes, in order to check the array radiation at different Talbot distances. Finally, the radiation provided by the array is picked up by a horn antenna, placed over the floor. This antenna is moved under the array, along the floor, in order to receive the temporal information of the array radiation as a function of space. For this purpose, a realtime oscilloscope (Agilent Infinium DS0871204B) is employed.

Figure 13 presents the magnitude of the field radiated by the described CRLH LWA array at the Talbot distance ($z_T=0.5483$ m), when the modulation frequency of the input pulse is set to $f_0=3.745$ GHz. As expected, complete reconstruction of the input spatial periodic distribution is obtained. The agreement between the experimental results and the simulation data is very good, especially considering the high sensitivity of the measuring system.

Finally, Fig. 14 presents the magnitude of the field radiated by the described CRLH LWA array at the fractional Talbot distance of $z_T/2=0.2874$ m, when the modulation frequency of the input pulse is set to $f_0=4.0$ GHz. As expected, double number of pulses is obtained, validating the tunable spatio-temporal Talbot phenomenon at fractional distances. The entire radiation has been shifted up in space due to the off-axis radiation. This effect is clearly apparent in this situation because a small number of antennas are employed. This spatial shift can be measured using Eq. (25), yielding $\Delta x=8.66$ cm.

V. CONCLUSIONS

A tunable spatio-temporal Talbot imaging phenomenon has been presented. This effect is based on the radiation properties of an array of beam-steered metamaterial CRLH LWAs, when all elements of the array are simultaneously excited by a modulated pulse. The scanning law property of these antennas has been exploited to obtain an off-axis radiation, which has led to the definition of a tunable Talbot distance, as a function of the input pulse modulation frequency. The proposed Talbot phenomenon has been analyzed theoretically, taking into account the aberrations produced by higher-order terms present in the free-space transfer function.

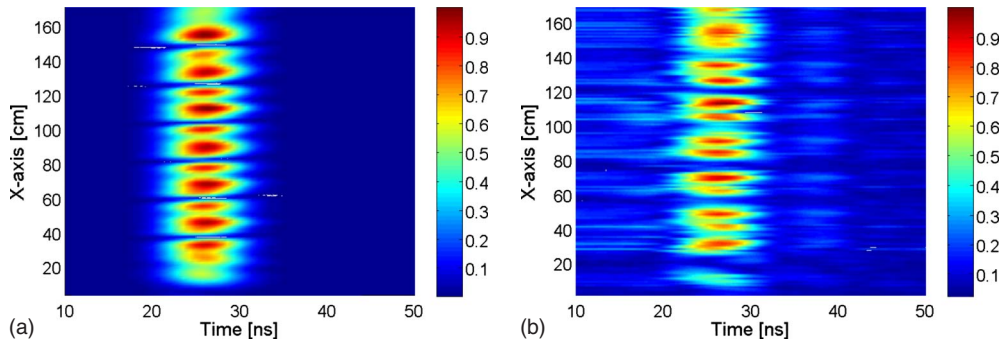

FIG. 14. (Color online) Normalized field (magnitude) radiated by an array of seven CRLH LWAs elements, excited by an input pulse with a modulation frequency of $f_0=4.0$ GHz at the fractional Talbot distance of $z_T/2=0.2874$ m. (a) Simulation results. (b) Measured data.

Then, numerical simulations have been employed to show the self-imaging and pulse multiplication effects and their variation as a function of frequency. Finally, experimental results have been presented to confirm the predicted phenomenon.

ACKNOWLEDGMENTS

This work was partially supported by the Spanish Ministry of Education and Science under Grant No. FPU-AP2006-015.

[1]H. F. Talbot, Philos. Mag. **9**, 401 (1836).
[2]J. Azaña and M. A. Muriel, IEEE J. Sel. Top. Quantum Electron. **7**, 728 (2001).
[3]A. W. Lohmann, Optik (Stuttgart) **79**, 41 (1987).
[4]L. Liu, Opt. Lett. **14**, 1312 (1989).
[5]J. Azaña and M. A. Muriel, Opt. Lett. **24**, 1672 (1999).
[6]N. K. Berger, B. Vodonos, S. Atkins, V. Smulakovsky, A. Bekker, and B. Fischer, Opt. Commun. **217**, 343 (2003).
[7]J. S. Gómez-Díaz, S. Gupta, A. Alvarez-Melcon, and C. Caloz, J. Appl. Phys. **104**, 104901 (2008).
[8]C. Caloz and T. Itoh, *Electromagnetic Metamaterials: Transmission Line Theory and Microwave Applications* (Wiley, New York/IEEE, New York, 2005).
[9]A. Oliner and D. R. Jackson, *Antenna Engineering Handbook*, 4th ed. (McGraw-Hill, New York, 2007).
[10]M. Testorf, J. Jahns, N. A. Khilo, and A. M. Goncharenko, Opt. Commun. **129**, 167 (1996).
[11]J. S. Gómez-Díaz, A. Álvarez-Melcón, and C. Caloz, in Proc. IEEE Antenna and Propagation Symposium, San Diego, 2008, pp. 1–4.
[12]J. S. Gómez-Díaz, A. Álvarez-Melcón, and C. Caloz, in Proc. IEEE Asia-Pacific Microwave Conference, Hong Kong, 2008, pp. 1–4.
[13]X. H. L. Zhou and C. Chan, Photonics Nanostruct. Fundam. Appl. **3**, 100 (2005).
[14]B. E. A. Saleh and M. C. Teich, *Fundamentals of Photonics*, 2nd ed. (Wiley-Interscience, New York, 2007).
[15]D. Pozar, *Microwave Engineering*, 3rd ed. (Wiley, New York, 2005).